The Growth of High-Crystalline Quality Mn_2Au (110) Thin Films

Daragh Mullarkey,[a] Daniel Casey, and Igor Shvets
School of Physics & CRANN, Trinity College, The University of Dublin

(Dated: 10 June 2022)

Mn_2Au is a bimetallic antiferromagnetic with an extraordinarily high Néel temperature of 1600 K. Mn_2Au has also been found to demonstrate Néel-order spin-orbit torque, allowing for electrical switching of the antiferromagnetic Néel vector. This has led to huge interest in this material for spintronic applications. Here we detail the growth of high quality Mn_2Au (110) thin films. The films were grown on a high quality Pt (111) buffer layer which was grown on an Al_2O_3 (0001) substrate. The Mn_2Au films have excellent crystalline quality as demonstrated by x-ray diffraction, x-ray reflection, and reflection high energy electron diffraction measurements. The Mn_2Au (110) films are found to grow with three equivalent in-plane rotation domains, caused by the Pt/Al_2O_3 substrate.

I. INTRODUCTION

Mn_2Au is an antiferromagnetic (AF) material with an extraordinarily high Néel temperature of approximately 1600 K[1,2]. The first study into the magnetic properties of this material used Mössbauer resonance, and indicated that the material was non-magnetic[3]. Further investigations into its magnetic properties later led to it being classified as possessing Pauli paramagnetism[4], however, first principle calculations later predicted the material to posses antiferromagnetic order[1]. Recent calculations predicted the easy axis for the Mn magnetic moments to lie along the [110] directions by calculating the magnetocrystalline anisotropy energy constants[5]. The easy axis was experimentally confirmed to lie in the basal plane of Mn_2Au[2] and subsequently found to lie along the predicted $\langle 110 \rangle$ directions[6]. Mn_2Au has a tetragonal crystal structure (crystallographic space group I4/mmm with magnetic space group Im'mm) with lattice parameters $a = 3.328$ Å and $c = 8.539$ Å[7]. This is shown schematically in Figure 4 (b)[8]. The magnetic structure is most easily understood by noting that each plane of Mn atoms perpendicular to the [001] direction is antiferromagnetically aligned with its neighbouring plane, above and below it. This magnetic structure can also be viewed as the Mn atoms lying on two separate, antiferromagnetically aligned sublattices. These two sublattices are inversion partners — an applied current will induce opposite inverse spin galvanic effects on both of these sublattices (known as the Néel-order spin-orbit torque, or NSOT[9]), allowing electrical switching of the antiferromagnetic Néel vector. The presence of this effect, its large spin orbit coupling[5],and the extremely high Néel temperature of Mn_2Au has led to it attracting great interest for use in antiferromagnetic spintronic devices.

The growth of Mn_2Au in thin film form was first demonstrated by Wu *et al.* in 2012. The Mn_2Au was grown by depositing alternating layers of Mn and Au via electron beam evaporation in an MBE which resulted in polycrystalline films with a (101) texture[10]. Mn_2Au with predominantly c-plane texture was obtained by growing the films on Al_2O_3 $(1\bar{1}02)$ via magnetron sputtering, both with[11,12] and without[13] a Ta (100) buffer layer. Growth of Mn_2Au with a single out of plane orientation was achieved by Zhou *et al.*, who grew Mn_2Au (103), (101), (204) on MgO (111), $SrTiO_3$ (100) , and MgO (200) respectively[14]. Here we detail a method for growing Mn_2Au (110) oriented thin films and their structural characterisation. As the $\langle 110 \rangle$ directions have been shown to be the easy directions in Mn_2Au, each magnetic domain within these (110) out-of-plane oriented films will possess one magnetic easy axis out-of-plane, while in the plane of the material there will be an easy axis and a hard axis separated by 90 degrees. Furthermore, the (110) surface of Mn_2Au is a pseudo-HCP (Hexagonal Close-Packed) surface, providing growth compatibility with other HCP materials which are commonly used in magnetic tunnel junction (MTJ) devices such as Pt (111) and Co (111)[15].

While Mn_2Au has been grown on a variety of substrate and buffer layer combinations (see Table I), each producing a variety of Mn_2Au film textures, the X-Ray Diffraction (XRD) data of many of the films produced shows the presence of multiple Mn_2Au phases which do not possess high crystalline quality. One material which is commonly used as a seed layer for the growth of magnetic structures is Pt, as it grows with high crystalline quality on Al_2O_3 (0001)[16] and can be utilised as an active part of a magnetic device in the form of Co/Pt multilayers, which present perpendicular magnetic anisotropy at specific Co layer thicknesses[17]. Pt has been shown to grow in the (111) orientation on the Al_2O_3 (0001) surface with 2 in-plane orientations domains[18]. The Pt (111) surface has a hexagonal surface unit cell with a surface lattice parameter of 2.774 Å, while the inter-atomic spacing on the Mn_2Au (110) surface varies from 2.747 Å to 2.852 Å, matching well with that of the Pt (111) surface. For this reason, we have chosen to use Pt as a seed layer for the growth of Mn_2Au on Al_2O_3.

[a] Electronic mail: mullarkd@tcd.ie

TABLE I. A summary of the thin film growth of Mn_2Au, showing the variety of substrate and buffer layer combinations which Mn_2Au can be grown on. The planes in the "Out-of-Plane Orientation" column are presented in order of XRD intensity. In the cases where a certain orientation has been demonstrated by multiple groups, only the first chronological instance is included.

Substrate	Buffer Layer	Growth Method	Out-of-Plane Orientation	Reference
MgO (001)	Fe (001)	MBE	(101) + (110) + (200)	[10]
Al_2O_3 ($1\bar{1}02$)	Ta (100)	Magnetron	(101) + (001)	[11]
Al_2O_3 ($1\bar{1}02$)	None	Magnetron	(001) + (200)	[13]
Si/SiO_2	Pt (111)	Magnetron	(110) + (112)	[13]
MgO (001)	ZrN (001)	Magnetron	(001) + (101)	[19]
MgO (111)	None	Magnetron	(103)	[14]
$SrTiO_3$ (100)	None	Magnetron	(101)	[14]
MgO (220)	None	Magnetron	(204)	[14]
Al_2O_3 ($1\bar{1}02$)	Ta (001)	Magnetron	(001) + (101)	[12]
Al_2O_3 ($1\bar{1}02$)	Ta (001)	MBE	(001)	[12]
Al_2O_3 (0001)	Pt (111)	MBE	(110)	This Work

II. EXPERIMENTAL DETAILS

Pt layers were deposited by e-beam evaporation in a DCA M600 MBE system with a base pressure of 2×10^{-10} Torr. Single crystal Al_2O_3 (0001) substrates were sonicated in isopropyl alcohol for 15 minutes before being inserted into the MBE for film growth. The Al_2O_3 substrates were annealed at 600 °C for one hour prior to deposition of the Pt. The Pt films were deposited at a rate of $0.05\,\text{Å}\,\text{s}^{-1}$ as determined by a calibrated quartz crystal monitor and the substrate was held at a temperature of 550 °C during growth. Details on the characterisation of the Pt films are given in the supplementary material[?] .

The Mn_2Au thin films were grown in the same growth chamber as was used to grow the Pt layers. For film growth, Mn and Au source material were evaporated simultaneously from separate Knudsen cells. The Au Knudsen cell was held at a temperature of 1282 °C, while the temperature of the Mn Knudsen cell was found to provide stoichiometric Mn_2Au at a temperature of 937 °C. These cell temperatures were found to provide Mn and Au atomic fluxes in a 2:1 ratio by growing separate Mn and Au films and measuring their thickness and density with X-Ray Reflectivity (XRR) and cross checking with a beam flux monitor located at the sample growth position. This resulted in an overall Mn_2Au growth rate of approximately $0.25\,\text{Å}\,\text{s}^{-1}$. For all samples, the substrate temperature was reduced to 250 °C from the Pt growth temperature of 550 °C upon completion of growth of the Pt seed layer. Simultaneously, the Knudsen cells were brought to their operating temperatures.

The stoichiometry of the Mn_2Au films was qualitatively assessed by analysing the XRD patterns of samples post-growth. When the Mn flux was too low MnAu phases could be seen in the XRD, while when the Mn flux was too high α-Mn would appear. This off-stoichiometric growth would be accompanied by a concomitant change in the RHEED, becoming a transmission-like pattern, indicative of island growth. Quantitative stoichiometric determination via X-ray Photoelectron Spectroscopy (XPS) was found to be unreliable; this is discussed in the supplementary material. A typical XRD pattern of a thick, stoichiometric $Mn_2Au/Pt/Al_2O_3$ film is shown in Figure S2 in the Supplementary material. Only the (110) phase of Mn_2Au is seen to be present.

III. RESULTS AND DISCUSSION

Figure 1 shows archetypal RHEED images after completion of each layer taken along the two Al_2O_3 high symmetry directions which are separated by 30°. An electron beam energy of 20 keV was used to produce all of the RHEED images shown here. The RHEED images of the Al_2O_3 substrate were taken at the annealing temperature of 600 °C, the images of the Pt layer were taken at the growth temperature of 550 °C, and those of the Mn_2Au layer were taken at room temperature. The measured streak spacings in the Al_2O_3 and Pt images were corrected for thermal expansion to their room temperature values[20,21]. This was found to only alter the measured spacings by an amount on the order of one pixel. The sharp diffraction spots seen along both directions of the Al_2O_3 substrate are indicative of a high quality single crystal surface, while the streaky nature of the RHEED patterns for the Pt and Mn_2Au layers indicate that they have flat surfaces consisting of grains or crystalline domains smaller than the coherence length of the electron beam[22].

The RHEED pattern shown here for the Mn_2Au layer is typically present after the growth of <5 nm of Mn_2Au and persists throughout growth, even in the thickest films grown (∼120 nm). Along the Al_2O_3 [$10\bar{1}0$] direction the Mn_2Au is seen to possess the same streak spacing as both the underlying Pt seed layer and the Al_2O_3 substrate, corresponding to the Al_2O_3 a lattice parameter; 4.758 Å.

While the oxygen sublattice of the Al_2O_3 surface appears to be in an HCP arrangement, it is only approximately so[23]. The slight deviations in the O atomic positions from those of the ideal HCP lattice results in the periodicity viewed along the Al_2O_3 [11$\bar{2}$0] direction being three atomic spacings, leading to the smaller RHEED streak spacing seen.

The Mn_2Au layer does appear to reproduce the same streak spacing as Al_2O_3, however, rather than being caused by a surface lattice which has distortions from the ideal HCP lattice positions, this reduced streak spacing is due to the presence of both Mn and Au on the Mn_2Au (110) surface. When viewed along the Al_2O_3 [11$\bar{2}$0] direction, the rows of atoms perpendicular to this direction, which are responsible for producing the symmetry in the RHEED pattern, contains both Mn and Au atoms. This is demonstrated in Figure 4 (a). This produces a periodicity equal to three times that of the inter-atomic spacing of the Mn_2Au surface, giving rise to a RHEED pattern which has the same streak spacing as Al_2O_3. However, When viewed along the Al_2O_3 [10$\bar{1}$0] direction, the perpendicular rows of atoms responsible for producing the RHEED pattern consist of only a single element and so the RHEED pattern appears identical to that of a monatomic HCP lattice, such as the Pt (111) surface. A schematic of the growth relations of Al_2O_3, Pt, and Mn_2Au is shown in Figure 4 (a). As the Pt layer does not show this reduced streak spacing along the [11$\bar{2}$0] direction it can be concluded that the Pt atoms form the expected HCP surface lattice rather than continuing the lateral symmetry of the underlying Al_2O_3 oxygen lattice. Post-annealing of the films in the growth chamber in UHV conditions at the Mn_2Au growth temperature of 250 °C was not found to have any impact on the surface quality of the films, as measured by RHEED. For this reason, the samples were cooled to room temperature upon completion of the growth of the Mn_2Au layer.

Figure 2 (a) shows an out of plane XRD scan for a 28.4 nm thick film on a 4.2 nm Pt seed layer on Al_2O_3 (0001) and Figure 2 (b) shows its corresponding XRR pattern, from which the layer thicknesses were obtained. The bulk positions of Mn_2Au (110) and Pt (111) are marked by dashed red and blue lines respectively and the Al_2O_3 (0006) peak is marked by an asterisk. The Mn_2Au (110) peak is found at a position of $2\theta = 38.159°$, compared to the bulk value of $2\theta = 38.213°$[7], giving $d_{110} = 2.357$ Å for our films. The Mn_2Au lattice thus shows a minimal out-of-plane expansion along the [110] direction by 0.14 %. The out of plane crystal relation of the layers determined from this measurement can be written as Al_2O_3 (0001)||Pt (111)||Mn_2Au(110). The inset shows a rocking curve measured at the Mn_2Au (110) peak. Fitting this peak to a pseudo-Voigt curve gives a Full Width at Half Maximum (FWHM) of the peak as 0.011° which is the resolution limit of the diffractometer used for the measurement. Such a narrow rocking curve is indicative of minimal mosaicity in the Mn_2Au film.

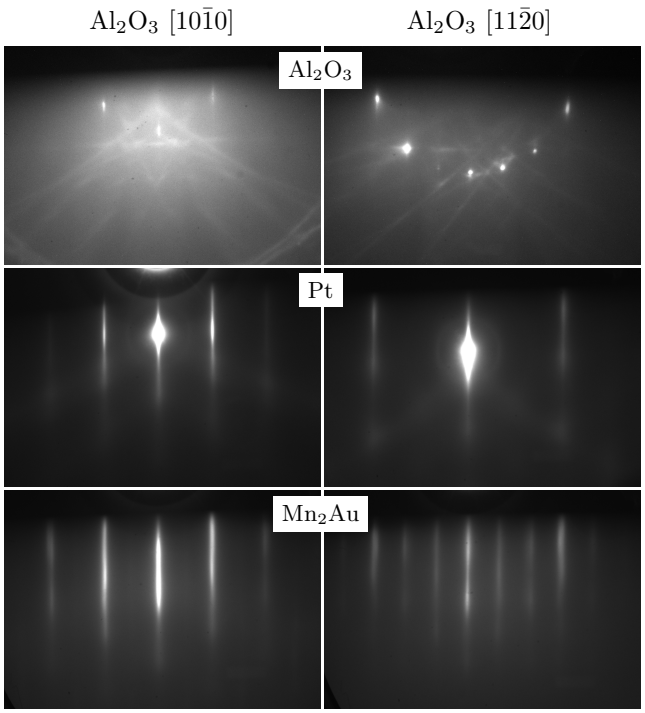

FIG. 1. RHEED images of a Mn_2Au/Pt/Al_2O_3 sample. Images were taken along the two high symmetry directions of the Al_2O_3 substrate: [10$\bar{1}$0] & [11$\bar{2}$0]. These two directions are separated by 30°.

The XRR fitting provides an estimate of the density of the Mn_2Au film of $11.0 \pm 0.3\,\mathrm{g\,cm^{-3}}$ which agrees well with the bulk value of $10.77\,\mathrm{g\,cm^{-3}}$. Both high frequency and low frequency oscillations in the XRD pattern from the Mn_2Au and Pt layers respectively are clearly visible, demonstrating the high crystalline quality of both layers in the sample. The Pendellösung fringe frequency gives estimates for the Mn_2Au and Pt out of plane crystalline thickness of 30 nm and 4 nm respectively, while the XRR fitting gives the layer thicknesses as 28.4 nm and 4.2 nm. The close agreement between these two values implies that both layers are a single crystalline domain throughout their thickness.

While the Pendellösung fringes of both the Mn_2Au and Pt layers show that the films are crystalline in the growth direction of the layers, it can not distinguish between the situation where the deposited films consist of a single in-plane rotation domain or multiple rotation domains. To find the in-plane epitaxial relation between the layers in Al_2O_3/Pt/Mn_2Au and to seek the presence of any rotation domains, azimuthal (ϕ) XRD scans were carried out. The scans were performed on a sample with a thick 120 nm Mn_2Au layer so as to enhance the signal from the weakly diffracting asymmetric peaks.

These ϕ-scans are shown in Figure 3. The Al_2O_3 substrate shows the expected three-fold symmetry. While the ϕ-scan of the Pt {100} planes would be expected to produce 3 peaks separated by 120° as the sample is

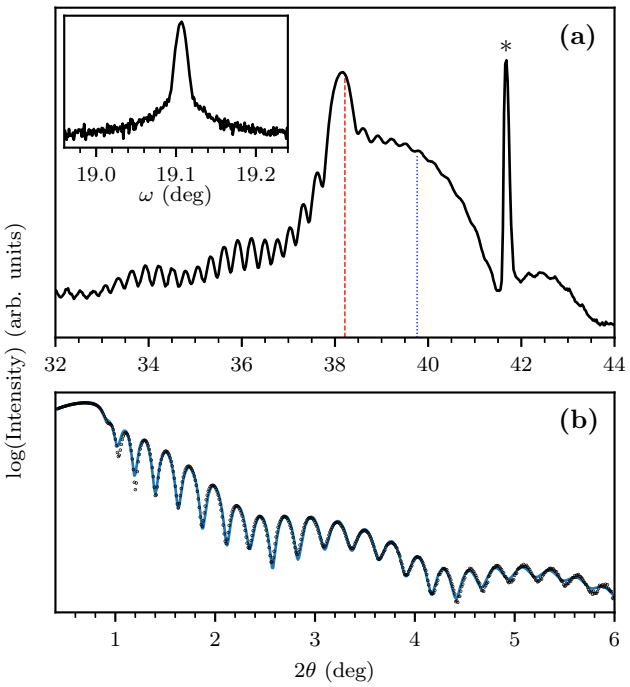

FIG. 2. (a) XRD of a 28.4 nm Mn_2Au/4.2 nm Pt film. The reference Mn_2Au (110) peak position is indicated by the red dashed line, while the Pt (111) position is indicated by the blue dotted line. The Al_2O_3 (0006) peak is indicated by an asterisk. The Pendellösung fringes provide an estimate of the coherent out of plane crystalline thickness of approximately 30 nm, indicating that the crystalline grains present in the film are continuous through the thickness of the film. Inset: A rocking curve of the Mn_2Au (110) peak with a FWHM of 0.011°. (b) XRR of a 28.4 nm Mn_2Au 4.2 nm Pt film. The black line and points are the data, and the blue line is the best fit to the data. The density of the Mn_2Au is estimated from the fitting as 11.0 g cm^{-3}.

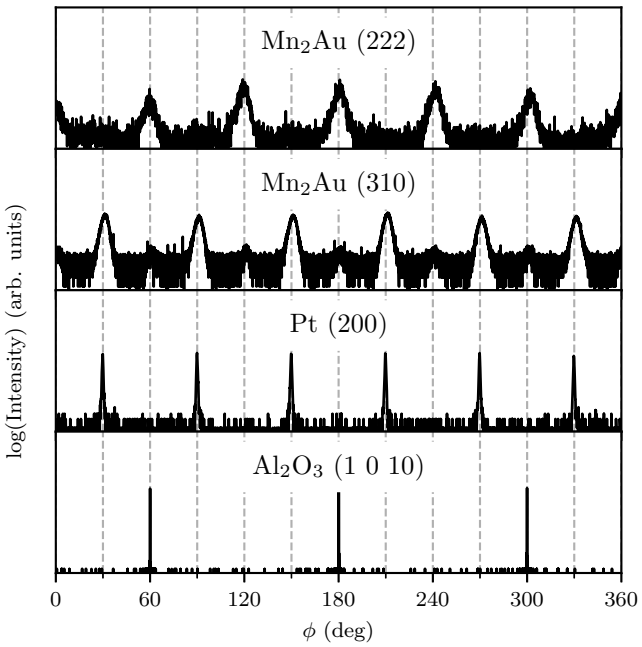

FIG. 3. Azimuthal (ϕ)-scans of the Al_2O_3 substrate (1 0 10) , the Pt buffer layer (100), and the Mn_2Au film (310) and (222) diffraction peaks demonstrating the in-plane relation between the layers.

rotated through 360°, 6 peaks are instead observed, implying that two domains, rotated by 60° with respect to each other, are present in the Pt buffer layers grown on Al_2O_3 (0001). The equal intensity of all six of the peaks suggests that these two domains are present in equal amounts across the sample. As the surface lattice of Pt (111) is hexagonal and thus possesses 6-fold symmetry, having both domains present will not affect the symmetry seen in RHEED measurements as they will appear equivalent; explaining their absence in both the RHEED images shown previously and in the previous work of Farrow *et al.*[18]. Similarly, the Mn_2Au ϕ-scan would be expected to only show 2 diffraction peaks due to the {310} planes, separated by 180°. As six peaks can be seen, this indicates that there are three equivalent domains present in the films, rotated by 60° with respect to each other. To confirm this, a ϕ scan was performed on a second Mn_2Au diffraction peak. The Mn_2Au (222) diffraction peak is expected to show the same two-fold symmetry as the (310) peaks, but with their positions rotated by 90° with respect to that of the (310) peaks. The same three equivalent rotation domains are indeed seen in this scan, with the expected 90° separation. The full out of plane epitaxial relation between the layers, as determined from XRD can be given as Al_2O_3 [0001]‖Pt [111]‖Mn_2Au [110], while the in-plane relation, as determined from RHEED and ϕ-scans is Al_2O_3 [11$\bar{2}$0]‖Pt [2$\bar{1}\bar{1}$]‖Mn_2Au [1$\bar{1}$1] or equivalently Al_2O_3 [10$\bar{1}$0]‖Pt [1$\bar{1}$0]‖Mn_2Au [001].

For use in future magnetic devices, Mn_2Au will be most useful as ultra thin films ($\leq$10 nm) in order to be able to reach the extremely high current densities needed for electrical switching of the magnetic order[24]. Reduction of the Mn_2Au thickness to this regime will also push the finite size Néel temperature towards room temperature from the extremely high bulk value of 1500 K, which is necessary for the thermal setting of exchange bias devices. To this end, the high quality MBE-grown Mn_2Au films demonstrated here show high promise for such size reduction, as they were found to grow with low roughness, minimal strain, and were found to consist of a single crystalline domain in the out of plane direction. We have compiled a table of all the various Mn_2Au thin film/substrate combinations as known to us in Table I. Our films are one of three works which were able to obtain Mn_2Au with only a single crystal phase present, and the first demonstration of single phase, (110) oriented films. While it is difficult to quantitatively estimate the effect that parastic crystalline phases in antiferromagnetic materials will have on devices constructed from these materials, previous work has demonstrated an increase in

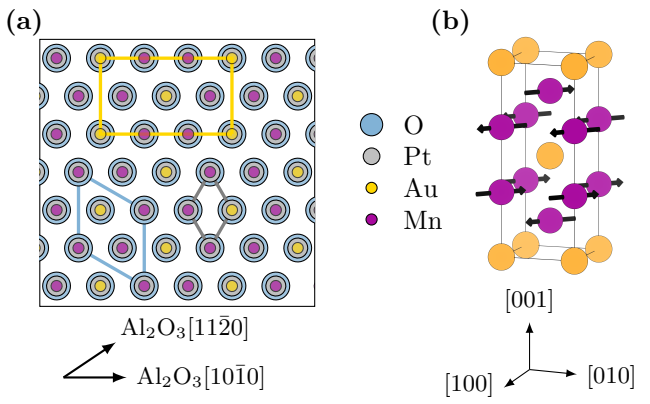

FIG. 4. (a) A plan view of the Mn_2Au (110) surface showing the physical growth relation between the Al_2O_3, Pt, and Mn_2Au layers. The surface unit cells of each are shown in blue, grey, and gold respectively. Only the oxygen sublattice of Al_2O_3 is shown, and the basis oxygen atoms are shown in the ideal HCP positions for clarity. (b) A single Mn_2Au unit cell. The black arrows on each Mn atom represent the direction of the atomic magnetic moment. Here they are pointing in the ⟨110⟩ magnetic easy directions. The antiferromagnetic alignment between Mn layers along the [001] axis is clearly seen.

the spin Hall angle with crystallinity of the archetype AF material IrMn. Zhang *et al.* showed that by using single crystal (111) samples of $IrMn_3$ rather than (111) textured polycrystalline samples , the spin Hall angle was found to increase by approximately 25 %[25].

Mn_2Au (110) films, in contrast to (001) oriented films are expected to have one out-of-plane easy axis (along [110]) and one in-plane easy axis (along [1-10]). This would need to be confirmed via X-ray Magnetic Linear Dichroism-Photoemission Electron Microscopy (XMLD-PEEM) or neutron diffraction measurements, as has been previously done for Mn_2Au (001) thin films[26]. This makes our (110) films unsuitable for NSOT measurements in the in-plane geometry previously used for (001) Mn_2Au films[27]. Additionally, the magnetic sublattices in Mn_2Au should be compensated for textured Mn_2Au (110). The compensated moments at the interface may make this orientation unfavourable for exchange bias and spin-orbitronic effects such as the Tunnelling Anisotropic Magnetoresistance (TAMR) effect. Further study needs to be done on our films to understand which model for exchange bias will apply to our compensated films (i.e., the models of Mieklejohn[28] or Malozemoff[29]). The HCP surface of the (110) films is highly compatible with other HCP and pseudo-HCP surface materials that are used in MTJ devices such as the Pt (111) shown here, and Fe (110) and Co (111) that we will show in future work (in preparation).

IV. CONCLUSION

To conclude, we have presented here the growth of high-crystalline quality, MBE-grown Mn_2Au (110) films which was made possible by the use of a Pt (111) buffer layer on an Al_2O_3 (0001) substrate. The out of plane and in plane epitaxial relation has been found to be Al_2O_3 [0001]‖Pt [111]‖Mn_2Au [110] and Al_2O_3 [11$\bar{2}$0]‖Pt [2$\bar{1}\bar{1}$]‖Mn_2Au [1$\bar{1}$1] respectively. The Mn_2Au layers show minimal strain compared to bulk lattice parameters, and grow with a low roughness and high crystalline quality, as evidenced by the Pendellösung fringes present in the XRD data.

V. SUPPLEMENTAL MATERIAL

See Supplemental Material for a discussion of the characterisation of Pt thin films, a large-range XRD scan of a Mn_2Au thin film, and a discussion on the stoichiometry of our Mn_2Au films.

ACKNOWLEDGMENTS

This research was supported by the Irish Research Council under grant number IRCLA/2019/171. D. C. acknowledges support of the Irish Research Council under grant number EPSPG/2017/329.

VI. AUTHOR DECLARATIONS

VII. CONFLICT OF INTEREST

The authors have no conflicts to disclose.

VIII. DATA AVAILABILITY

The data that support the findings of this study are available from the corresponding author upon reasonable request.

[1] S. Khmelevskyi and P. Mohn, "Layered antiferromagnetism with high Néel temperature in the intermetallic compound Mn_2Au," Applied Physics Letters **93**, 162503 (2008).
[2] V. Barthem, C. Colin, H. Mayaffre, M.-H. Julien, and D. Givord, "Revealing the properties of Mn_2Au for antiferromagnetic spintronics," Nature communications **4** (2013).
[3] G. Longworth and B. Window, "Mössbauer studies of gold manganese alloys," Journal of Physics F: Metal Physics **1**, 217 (1971).
[4] S. Abe, M. Matsumoto, T. Kaneko, H. Yoshida, H. Morita, and T. Kanomata, "Magnetic properties of ordered alloy $AuMn_2$," Journal of magnetism and magnetic materials **140**, 103 (1995).
[5] A. B. Shick, S. Khmelevskyi, O. N. Mryasov, J. Wunderlich, and T. Jungwirth, "Spin-orbit coupling induced anisotropy effects in bimetallic antiferromagnets: A route towards antiferromagnetic spintronics," Physical Review B **81**, 212409 (2010).

[6] V. M. Barthem, C. V. Colin, R. Haettel, D. Dufeu, and D. Givord, "Easy moment direction and antiferromagnetic domain wall motion in Mn_2Au," Journal of Magnetism and Magnetic Materials **406**, 289 (2016).

[7] P. Wells and J. Smith, "The structure of Mn_2Au and Mn_3Au," Acta Crystallographica Section A: Crystal Physics, Diffraction, Theoretical and General Crystallography **26**, 379 (1970).

[8] K. Momma and F. Izumi, "VESTA 3 for three-dimensional visualization of crystal, volumetric and morphology data," Journal of Applied Crystallography **44**, 1272 (2011).

[9] J. Železnỳ, H. Gao, K. Vỳbornỳ, J. Zemen, J. Mašek, A. Manchon, J. Wunderlich, J. Sinova, and T. Jungwirth, "Relativistic Néel-order fields induced by electrical current in antiferromagnets," Physical Review Letters **113**, 157201 (2014).

[10] H.-C. Wu, Z.-M. Liao, R. Sofin, G. Feng, X.-M. Ma, A. B. Shick, O. N. Mryasov, and I. V. Shvets, "Mn_2Au: Body-centered-tetragonal bimetallic antiferromagnets grown by molecular beam epitaxy," Advanced Materials **24**, 6374 (2012).

[11] M. Jourdan, H. Bräuning, A. Sapozhnik, H. Elmers, H. Zabel, and M. Kläui, "Epitaxial Mn_2Au thin films for antiferromagnetic spintronics," Journal of Physics D: Applied Physics **48**, 385001 (2015).

[12] S. P. Bommanaboyena, T. Bergfeldt, R. Heller, M. Kläui, and M. Jourdan, "High quality epitaxial Mn_2Au (001) thin films grown by molecular beam epitaxy," Journal of Applied Physics **127**, 243901 (2020).

[13] M. Arana, F. Estrada, D. S. Maior, J. B. S. Mendes, L. E. Fernandez-Outon, W. A. A. Macedo, V. M. T. S. Barthem, D. Givord, A. Azevedo, and S. M. Rezende, "Observation of magnons in Mn_2Au films by inelastic brillouin and raman light scattering," Applied Physics Letters **111**, 192409 (2017).

[14] X. Zhou, J. Zhang, F. Li, X. Chen, G. Shi, Y. Tan, Y. Gu, M. Saleem, H. Wu, F. Pan, and C. Song, "Strong orientation-dependent spin-orbit torque in thin films of the antiferromagnet Mn_2Au," Physical Review Applied **9**, 054028 (2018).

[15] B. G. Park, J. Wunderlich, X. Martí, V. Holý, Y. Kurosaki, M. Yamada, H. Yamamoto, A. Nishide, J. Hayakawa, H. Takahashi, A. B. Shick, and T. Jungwirth, "A spin-valve-like magnetoresistance of an antiferromagnet-based tunnel junction," Nature Materials **10**, 347 (2011).

[16] O. Benamara, E. Snoeck, M. Respaud, and T. Blon, "Growth of platinum ultrathin films on Al_2O_3 (0001)," Surface Science **605**, 1906 (2011).

[17] C.-J. Lin, G. Gorman, C. Lee, R. Farrow, E. Marinero, H. Do, H. Notarys, and C. Chien, "Magnetic and structural properties of Co/Pt multilayers," Journal of Magnetism and Magnetic Materials **93**, 194 (1991).

[18] R. Farrow, G. Harp, R. Marks, T. Rabedeau, M. Toney, D. Weller, and S. Parkin, "Epitaxial growth of pt on basal-plane sapphire: a seed film for artificially layered magnetic metal structures," Journal of Crystal Growth **133**, 47 (1993).

[19] M. Meinert, D. Graulich, and T. Matalla-Wagner, "Electrical switching of antiferromagnetic Mn_2Au and the role of thermal activation," Physical Review Applied **9**, 064040 (2018).

[20] R. K. Kirby, "Platinum — a thermal expansion reference material," International Journal of Thermophysics **12**, 679 (1991).

[21] B. Yates, R. F. Cooper, and A. F. Pojur, "Thermal expansion at elevated temperatures. II. aluminium oxide: experimental data between 100 and 800 k and their analysis," Journal of Physics C: Solid State Physics **5**, 1046 (1972).

[22] S. Hasegawa, "Reflection high-energy electron diffraction," (2012) pp. 1–14.

[23] M. Kronberg, "Plastic deformation of single crystals of sapphire: Basal slip and twinning," Acta Metallurgica **5**, 507 (1957).

[24] P. Wadley, B. Howells, J. elezny, C. Andrews, V. Hills, R. P. Campion, V. Novak, K. Olejnik, F. Maccherozzi, S. S. Dhesi, S. Y. Martin, T. Wagner, J. Wunderlich, F. Freimuth, Y. Mokrousov, J. Kune, J. S. Chauhan, M. J. Grzybowski, A. W. Rushforth, K. W. Edmonds, B. L. Gallagher, and T. Jungwirth, "Electrical switching of an antiferromagnet," Science **351**, 587 (2016).

[25] W. Zhang, W. Han, S.-H. Yang, Y. Sun, Y. Zhang, B. Yan, and S. S. P. Parkin, "Giant facet-dependent spin-orbit torque and spin hall conductivity in the triangular antiferromagnet $IrMn_3$," Science Advances **2**, e1600759 (2016).

[26] A. A. Sapozhnik, M. Filianina, S. Y. Bodnar, A. Lamirand, M.-A. Mawass, Y. Skourski, H.-J. Elmers, H. Zabel, M. Kläui, and M. Jourdan, "Direct imaging of antiferromagnetic domains in Mn_2Au manipulated by high magnetic fields," Physical Review B **97**, 134429 (2018).

[27] S. Y. Bodnar, L. Šmejkal, I. Turek, T. Jungwirth, O. Gomonay, J. Sinova, A. A. Sapozhnik, H.-J. Elmers, M. Kläui, and M. Jourdan, "Writing and reading antiferromagnetic Mn_2Au by Néel spin-orbit torques and large anisotropic magnetoresistance," Nature Communications **9** (2018), 10.1038/s41467-017-02780-x.

[28] W. H. Meiklejohn, "Exchange anisotropy—a review," Journal of Applied Physics **33**, 1328–1335 (1962).

[29] A. P. Malozemoff, "Random-field model of exchange anisotropy at rough ferromagnetic-antiferromagnetic interfaces," Physical Review B **35**, 3679–368 (1987).